nature communications

Article

https://doi.org/10.1038/s41467-025-66642-7

Porous organic cage mixed matrix membranes for efficient enantioseparation

Received: 8 April 2025

Accepted: 12 November 2025

Published online: 28 November 2025

Check for updates

Yifan Li[1], Zheng Liu[1], Daojiang Zhu[1], Yuan Xia[1], Bin Wu[2], Tingting Xu[1] ✉, Xingya Li[1] ✉ & Tongwen Xu[1] ✉

Mixed matrix membranes (MMMs) based on homochiral microporous materials have emerged as a promising approach for enantioselective separation. However, constructing MMMs for achieving efficient enantioselective separation at a high feed concentration still remains a great challenge due to the suboptimal interfacial compatibility. Here, we employ soluble porous organic cages (POCs) of intrinsic chiral sites as fillers to fabricate MMMs devoid of interfacial defects, exhibiting fast and selective enantioseparation for racemic 2-phenylpropionic acid with a flux of 2.93×10^{-3} mol m^{-2} h^{-1} and an enantiomeric excess (ee) value up to 100% at a high concentration of 0.1 mol L^{-1}. The POC-based MMMs demonstrate a long-term operation stability with a low ee decline rate of 0.56% h^{-1}. This work reveals the imperative role of the microporous chiral environment in POCs for the enantioselective recognition and furnishes guidelines for the construction of POC-based membranes for efficient chiral separation.

The fast and selective separation of enantiomers is significant in the pharmaceutical, agrochemical, and food additive industries[1–3]. Membrane-based enantioselective separation offers a promising approach for chiral separation with the advantages of low energy consumption, continuous operation, and scalability[4–7]. Homochiral microporous materials, such as homochiral metal-organic frameworks (MOFs) and covalent organic frameworks (COFs), are regarded as a promising membrane material for chiral separations due to their high porosity, tunable chiral pore environment, and diverse structures[8–17]. Although a number of polycrystalline membranes based on homochiral microporous materials were developed, the complex preparation process and fragile property have impeded the production of membranes and their applications in chiral separation[18–22]. Alternatively, mixed matrix membranes (MMMs) combine the enantioselective separation capability of homochiral microporous materials with the processability of polymer matrices, providing a facile method for preparing chiral separation membranes[6,23]. Recently, a variety of MMMs based on homochiral microporous materials (e.g., MOFs and COFs) have been developed[24–27]. However, MOFs and COFs showcase a poor compatibility with the polymer matrix due to the absence of solution processability, resulting in unavoidable interfacial defects in MMMs[28,29]. The presence of interfacial defects in MMMs accelerates the diastereoselective diffusion and decreases the enantioselectivity with increasing feed concentrations[5,26]. Up to date, almost all the recorded MMMs are only capable of achieving enantioselective separation at low feed concentrations (i.e., 10^{-3}–10^{-2} mol L^{-1})[23,25,26]. Therefore, it is highly desirable to construct MMMs without interfacial defects to achieve enantioselective separation at high feed-concentration scenarios.

Porous organic cages (POCs) are microporous materials with permanent channels composed of internal cavities and open windows to allow the penetration of guest molecules[30–32]. Homochiral POCs are synthesized from chiral diamine and aldehyde monomers by a condensation reaction[33,34]. They contain abundant and uniformly distributed chiral sites within cavities, enabling them to realize the selective recognition and separation of enantiomers[35–37]. Additionally, different from MOFs and COFs, these cages possess good solution processability and filler-polymer interfacial compatibility, rendering them ideal fillers for MMMs[29,38]. CC3 is a well-known homochiral POC that has been proven as a promising candidate for chiral

[1]Key Laboratory of Precision and Intelligent Chemistry, School of Chemistry and Materials Science, University of Science and Technology of China, Hefei, China. [2]School of Chemistry & Chemical Engineering, Key Laboratory of Environment-Friendly Polymeric Materials of Anhui Province, Anhui University, Hefei, China. ✉e-mail: xutt49@ustc.edu.cn; xingyali@ustc.edu.cn; twxu@ustc.edu.cn

separation[39,40]. Wang et al. prepared composite enantioselective membranes based on homochiral POC (CC3-R) by interfacial polymerization, where CC3-R crystals were dispersed in the aqueous phase and finally trapped and entangled by polyamide chains. The resulting CC3-R/PA membrane presented an enantioselectivity for racemic limonene at a concentration of 1.0×10^{-2} mol L^{-1}, with a flux of 7.30×10^{-4} mol m^{-2} h^{-1} and an ee value of 95.2%[41]. Although this study suggests the potential of homochiral CC3-R in the field of enantioselective separations, the solution processability of POCs has not been employed. CC3-R in the crystal form was embedded in the polyamide matrix, which might result in uneven distribution of chiral sites, thereby compromising the separation performance. In addition, the selective recognition mechanism of POCs for enantiomers has not been subjected to further investigation.

Herein, we deploy the inherent chirality and solution processibility of POC to fabricate homochiral MMMs for enantioseparation. The homochiral POC crystals (i.e., CC3-R, CC4-R, and CC19-R) and the protonated poly (alkyl-biphenyl pyridinium) (HPABP) matrix were homogeneously dissolved via the co-solvent method. The synthesized membranes are free of interfacial defects, and POC crystals are uniformly distributed in the polymeric matrix. CC3-HPABP and CC4-HPABP membranes show superior enantioselectivity for racemic 2-phenylpropionic acid, with the highest ee value up to 100% (R-enantiomer in excess). But the CC19-HPABP membrane displays diastereoselectivity for racemic 2-phenylpropionic acid. Theoretical calculations indicate that the enantioselectivity stems from specific hydrogen bonding interactions between the enantiomer and the chiral sites in CC3-R and CC4-R, whereas strong hydrogen bonding between the enantiomer and the achiral hydroxyl group within the CC19-R pore disrupts the specific interactions with the chiral sites. The CC3-HPABP-15% membrane shows fast and selective enantioseparation for racemic 2-phenylpropionic acid at a high concentration of 0.1 mol L^{-1}. Furthermore, the membrane demonstrates a long-term operation stability with a high ee above 80% for 36 h.

Results

Preparation and characterization of POC mixed matrix membranes

The studied homochiral POCs (i.e., CC3-R, CC4-R, and CC19-R) were synthesized by imine condensation reactions between aldehydes and chiral diamines, which possess a window-cavity structure of similar sizes but exhibit different microporous chiral environments (Fig. 1a and Supplementary Figs. 1 and 2)[42,43]. The X-ray diffraction (XRD) patterns and Fourier-transform infrared (FT-IR) spectra confirm the successful synthesis of the POCs (Supplementary Fig. 3a, b). Circular dichroism (CD) spectroscopy verifies the homochirality of the POCs (Supplementary Fig. 3c). The porosity of POCs was determined through nitrogen adsorption-desorption experiments. The results suggest that POCs have two major pore size distributions around 7 Å and 11 Å, corresponding to the triangular windows and internal tetrahedral cavities, respectively (Supplementary Fig. 4). As shown in Fig. 1, the POC-based MMMs are composite and porous membranes, fabricated by dissolving POC crystals and HPABP polymer in the co-solvent of dichloromethane and methanol. Since POCs possess significantly negative potentials deriving from the N atom and π electrons on the benzene ring[44], while the pyridine group of HPABP is positively charged, the electrostatic attraction interactions between POCs and HPABP can effectively promote the uniform dispersion of POCs within the polymer matrix and diminish interfacial defects (Supplementary Figs. 5–7). The good solubility and processability of POCs enable the evenly dispersed POC crystals in the polymer matrix (Supplementary Fig. 8). Besides, dynamic light scattering (DLS) measurements indicated that the hydrodynamic diameters of CC3-R, CC4-R, and CC19-R dissolved in the co-solvent were approximately 1.66 nm, 1.62 nm, and 1.80 nm, respectively, which coincide with the molecular size of POC (Supplementary Fig. 9). This implies that POC is disassembled into discrete molecular cages rather than aggregated crystals in the co-solvent. Therefore, POC can be uniformly dispersed in the polymer matrix via the co-solvent method, forming MMMs without interfacial defects[38,45]. After casting the membrane solution and solvent evaporation, the MMMs with various POC loadings (5 wt%, 15 wt%, and 30 wt%) were successfully fabricated, validated by scanning electron microscopy (SEM) images of the surface and cross-section (Fig. 1b and Supplementary Figs. 10–14). At low POC loadings (i.e., 5 and 15 wt%), the surface images show a uniform and smooth surface without any visible defects, indicating a good compatibility between POC and HPABP matrix. The cross-sectional images display a similar and uniform thickness of ~60 μm, and no visible POC crystals are observed in the MMMs. However, with POC loading increasing, the POC crystals appear in both surface and cross-sectional images of MMMs. The Raman mapping images of MMMs reveal the presence and uniform distribution of POC in the HPABP matrix, compared to the original

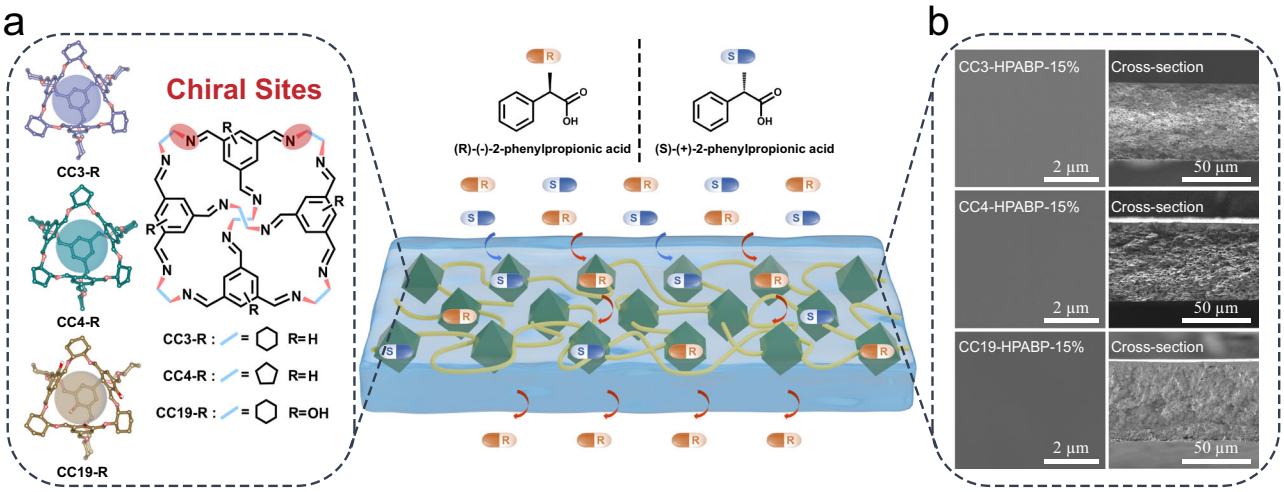

Fig. 1 | A representation of POC-based mixed matrix membranes for the selective transport of R-2-phenylpropionic acid molecules from a racemic mixture. CC3-HPABP and CC4-HPABP membranes display an enantioselectivity for racemic 2-phenylpropionic acid, whereas CC19-HPABP membrane shows a diastereoselectivity for racemic 2-phenylpropionic acid. **a** The three POCs possess a window-cavity structure of similar sizes, where CC3-R and CC19-R have hexagonal amine monomer and CC4-R with pentagonal amine monomer, and CC19-R has extra hydroxyl sites, forming different microporous chiral environments. **b** Surface and cross-sectional scanning electron microscopy (SEM) images of POC-based mixed matrix membranes.

https://doi.org/10.1038/s41467-025-66642-7

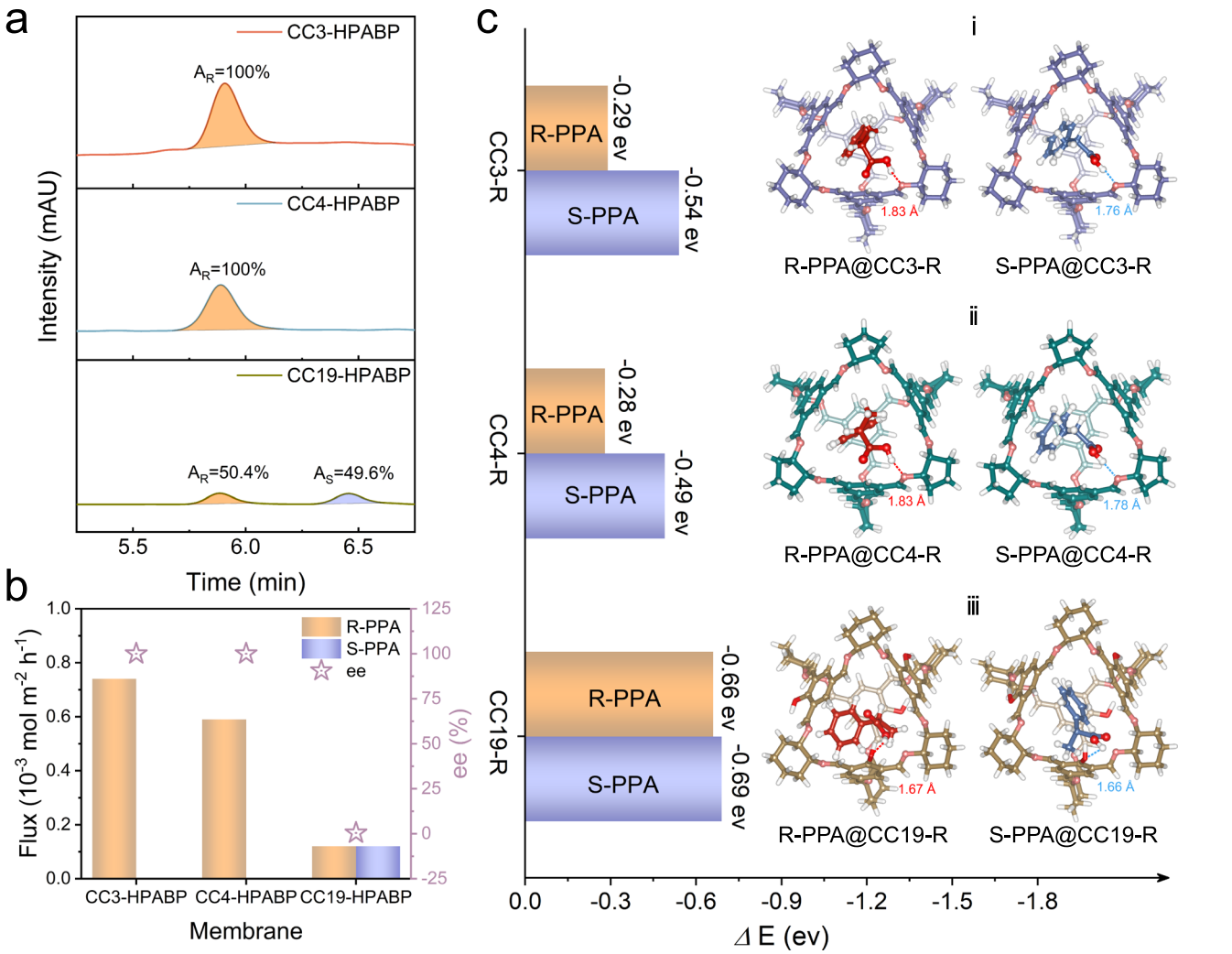

Fig. 2 | Enantioselective separation mechanism of POC mixed matrix membranes. a HPLC spectra of 2-phenylpropionic acid enantiomers after separation for 2 h with POC-based MMMs. **b** Flux and enantiomeric excess (ee) of POC-based MMMs. **c** The host-guest interactions of R-PPA@CC3-R, S-PPA@CC3-R (i), R-PPA@CC4-R, S-PPA@CC4-R (ii), R-PPA@CC19-R and S-PPA@CC19-R (iii) based on theoretical calculations. The values of ΔE represent the binding energies between the chiral molecules and POCs. The labeled distances denote the hydrogen bond lengths.

HPABP membrane (Supplementary Fig. 15). Atomic force microscopy (AFM) images reveal a smooth and flat membrane surface with low surface roughness (Supplementary Fig. 16 and Supplementary Table 1). Compared to the HPABP membrane, FT-IR spectra of MMMs show an absorption peak of C=N at 1699 cm^{-1} corresponding to the characteristic group of POCs (Supplementary Fig. 17)[38].

Enantioselective separation mechanism of POC mixed matrix membranes

The enantioselective separation performance of POC-MMMs was evaluated under concentration gradient driven by a homemade apparatus, and the 2-phenylpropionic acid was selected as the target molecule. Specifically, the racemic 2-phenylpropionic acid/ethanol solution and blank ethanol solution were used as the feed and permeate solution, respectively. The high-performance liquid chromatography (HPLC) analysis of the permeate solution was conducted to determine the concentration of the R- and S-enantiomers (Supplementary Figs. 18–21). The enantioselective performances (i.e., flux and ee) of the MMMs were further calculated from the above results. To investigate the effect of POC loading on the chiral separation performance of the MMMs, all MMMs (i.e., CC3-HPABP, CC4-HPABP, and CC19-HPABP) were tested under the same conditions with permeation time of 2 h under 0.001 mol L^{-1} racemic 2-phenylpropionic acid (Fig. 2a, b and Supplementary Figs. 22–24). For CC3-HPABP membranes, a notable and substantial increase in the fluxes is observed as the loading of CC3-R progressively increases (Supplementary Fig. 22c). As shown in Supplementary Fig. 22d, the ee values of the CC3-HPABP membranes drop from 100% to 91.8% with the increase in CC3-R loading from 5/15 to 30 wt%. This decline could be attributed to the partial aggregation of CC3-R during the membrane fabrication process, resulting in the formation of non-selective diffusion pathways within the membrane, which diminishes the enantioselectivity (Supplementary Fig. 11). The same case happens in CC4-HPABP membranes, as shown in Supplementary Fig. 23. However, all CC19-HPABP membranes exhibit diastereoselectivity toward 2-phenylpropionic acid (Supplementary Fig. 24). Based on the results of the effect of POC loading on the chiral separation performance of MMMs, the optimal POC loading (i.e., 15 wt%) was determined for subsequent studies.

To confirm that the chiral separation capability of the MMMs is attributed to the addition of the homochiral POCs and exclude the effect of the polymer matrix, the enantioselective separation test of the HPABP membrane was performed. As shown in Supplementary Fig. 25, the peak areas of R-2-phenylpropionic acid and S-2-phenylpropionic acid through the HPABP membrane are nearly

equivalent, suggesting that the HPABP membrane has little effect on the enantioselectivity of racemic 2-phenylpropionic acid. Furthermore, the ethanol contact angle tests of the three POCs indicate their similar affinity to ethanol. Therefore, when investigating differences in chiral separation performance, the influence of the hydroxyl group in CC19-R on solvent affinity can be negligible (Supplementary Fig. 26).

To study the interaction disparity among the three POCs, density functional theory (DFT) calculations were employed to evaluate the binding energy between the chiral sites of POCs and the enantiomer 2-phenylpropionic acid. The calculated binding energy (Fig. 2c-i and Supplementary Fig. 27) of CC3-R to S-2-phenylpropionic acid (i.e., −0.54 eV) is significantly higher than that to R-2-phenylpropionic acid (i.e., −0.29 eV), indicating a stronger affinity with S-2-phenylpropionic acid. The binding energy difference lies in the varying hydrogen bonding interactions between the carboxyl groups in the 2-phenylpropionic acid and the nitrogen atoms in the CC3-R. During the separation process, the uniformly distributed CC3-R crystals in the membrane preferentially adsorb S-2-phenylpropionic acid through the stronger binding affinity between the chiral recognition sites and the enantiomers. The adsorbed S-2-phenylpropionic acid molecules are retained in the membrane, whereas R-2-phenylpropionic acid molecules permeate through the membrane more easily due to their lower affinity to the chiral recognition sites. The affinity difference between R- and S-2-phenylpropionic acid leads to a high enantioselective separation. The same case happens in CC4-R, as shown in Fig. 2c-ii and Supplementary Fig. 28. Therefore, the CC4-HPABP membrane also delivers a decent enantioselectivity. However, the calculated binding energies (Fig. 2c-iii and Supplementary Fig. 29) of CC19-R to R- and S-2-phenylpropionic acid are roughly identical, resulting in a non-selective recognition of CC19-R with both R- and S-2-phenylpropionic acid. Compared to CC3-R and CC4-R, CC19-R displays structural differences primarily due to the presence of non-chiral hydroxyl groups in the internal cavities. The hydroxyl group in CC19-R forms a stronger hydrogen bonding interaction with the carboxyl group in 2-phenylpropionic acid, which disrupts the hydrogen bonding interactions between the carboxyl group in 2-phenylpropionic acid and the nitrogen atom in CC19-R. The non-specific hydrogen bonding interaction enables CC19-R to generate comparable binding affinities for R- and S-2-phenylpropionic acid, thus interfering with the selective recognition of the enantiomers. Consequently, the adsorption of CC19-R for R- and S-2-phenylpropionic acid is non-selective during membrane separation, which ultimately induces the diastereoselective separation of R- and S-2-phenylpropionic acid for the CC19-HPABP membrane. Meanwhile, the stronger hydrogen bonding effect causes a higher binding energy for CC19-R with R- and S-2-phenylpropionic acid than that of CC3-R and CC4-R. As a result, CC19-HPABP-15% membrane shows a lower flux (i.e., 1.20×10^{-4} mol m^{-2} h^{-1}) than that of CC3-HPABP-15% (i.e., 7.40×10^{-4} mol m^{-2} h^{-1}) and CC4-HPABP-15% (i.e., 5.90×10^{-4} mol m^{-2} h^{-1}) membranes (Fig. 2b). Additionally, molecular dynamics (MD) simulations were performed to further confirm the difference in diffusivity of R- and S-2-phenylpropionic acid enantiomers within POCs (Supplementary Fig. 30). The results reveal that the diffusion coefficient (D) of R-PPA enantiomer in CC3-R is higher than that of S-PPA, whereas the diffusion coefficients of the two enantiomers in CC19-R are quite close, both lower than those of R-PPA in CC3-R (Supplementary Fig. 30c). The theoretical simulations reveal the key role of the microporous chiral environments derived from POCs in the enantioselective separation of enantiomers.

The adsorption properties of three POCs to 2-phenylpropionic acid were also examined to verify the affinity difference (Supplementary Fig. 31). The adsorption results indicate that CC3-R and CC4-R crystals have a preference for adsorbing the S-2-phenylpropionic acid over the R-2-phenylpropionic acid, while the adsorption of R-2-phenylpropionic acid for CC19-R is basically equal to the adsorption of S-2-phenylpropionic acid. These results are consistent with those from the theoretical simulations. Based on the above results, a reasonable enantioselective separation mechanism can be elaborated in the studied MMMs (Supplementary Fig. 32). The chiral separation in CC3-HPABP and CC4-HPABP membranes is primarily based on a retarded transport mechanism[5]. The CC3-R and CC4-R selectively absorb S-2-phenypropionic acid through the strong binding affinity and retain the absorbed S-2-phenypropionic acid in the membrane, while the R-2-phenypropionic acid can diffuse more easily through the membrane due to a lower binding affinity.

Enantioselective separation of CC3-HPABP-15% membrane at a high feed concentration

As a high-concentration condition is challenging for the membrane-based chiral separation process, a high concentration (i.e., 0.1 mol L^{-1}) of the feed solution was used to perform separation tests. Figure 3a shows the HPLC results of the permeate solution for CC3-HPABP-15% membrane over time, where the enantiomeric peaks with different intensities were observed. The area ratio of R-2-phenylpropionic acid peak is 100% and the signal of S-2-phenylpropionic acid cannot be detected as the permeation proceeds 15 min. The result indicates that CC3-HPABP-15% membrane retains all of the S-2-phenylpropionic acid molecules and allows the R-2-phenylpropionic acid molecules to pass through, leading to an ee of 100%. The peak area of the R-2-phenylpropionic acid consistently exceeds that of the S-2-phenylpropionic acid during the whole permeation test, revealing the superior enantioselectivity for 2-phenylpropionic acid of CC3-HPABP-15% membrane at such a high feed concentration. The flux of R-2-phenylpropionic acid reached 2.93×10^{-3} mol m^{-2} h^{-1} at the initial stage of the separation process (15 min) and gradually decreased to 1.62×10^{-3} mol m^{-2} h^{-1} after 1 h of separation, while the flux of S-2-phenylpropionic acid stayed at a low value (Fig. 3b). Moreover, the CC3-HPABP-15% membrane keeps a high ee above ~90% during the first hour of separation (Fig. 3c). Therefore, the rapid and efficient enantioselective separation of the 2-phenylpropionic acid is achieved with the CC3-HPABP-15% membrane at such a high feed concentration, which has not been reported in the literature.

Enantioselective separation stability of CC3-HPABP-15% membrane

To evaluate the stability of CC3-HPABP-15% membrane, a long-term (36 h) separation test was conducted at a concentration of 0.001 mol L^{-1} 2-phenylpropionic acid solution. The HPLC results show that the area values of R-2-phenylpropionic acid are consistently much higher than those of S-2-phenylpropionic acid during the continuous measurement (Fig. 4a–d). The flux of R-2-phenylpropionic acid is measured to be 5.10×10^{-4} mol m^{-2} h^{-1} at 4 h, which gradually decreases to 2.40×10^{-4} mol m^{-2} h^{-1} after 12 h of separation and then remains relatively stable (Fig. 4e). In contrast, the flux of S-2-phenylpropionic acid displays a slight upward trend and then remains at a lower value. The enantioselectivity of CC3-HPABP-15% membrane drops slowly with permeation time, remaining at 100% ee at 4 h and gradually decreasing to 81% after 36 h (Fig. 4f). This decline can be attributed to the selective adsorption of S-2-phenylpropionic acid by the chiral recognition sites of the CC3-R crystals within the membrane. As the permeation time increases, these chiral recognition sites are progressively occupied by adsorbed S-2-phenylpropionic acid, reducing the number of available chiral recognition sites and consequently leading to a decline in enantioselectivity.

Effect of concentration gradient on enantioselective separation of CC3-HPABP-15% membrane

To evaluate the effect of the feed concentration on the chiral separation performance of the CC3-HPABP-15% membrane, racemic 2-phenylpropionic acid feed solution with four different concentrations (0.001, 0.01, 0.05, and 0.1 mol L^{-1}) was examined (Supplementary Figs. 33-35). The fluxes as a function of time for R- and S-2-

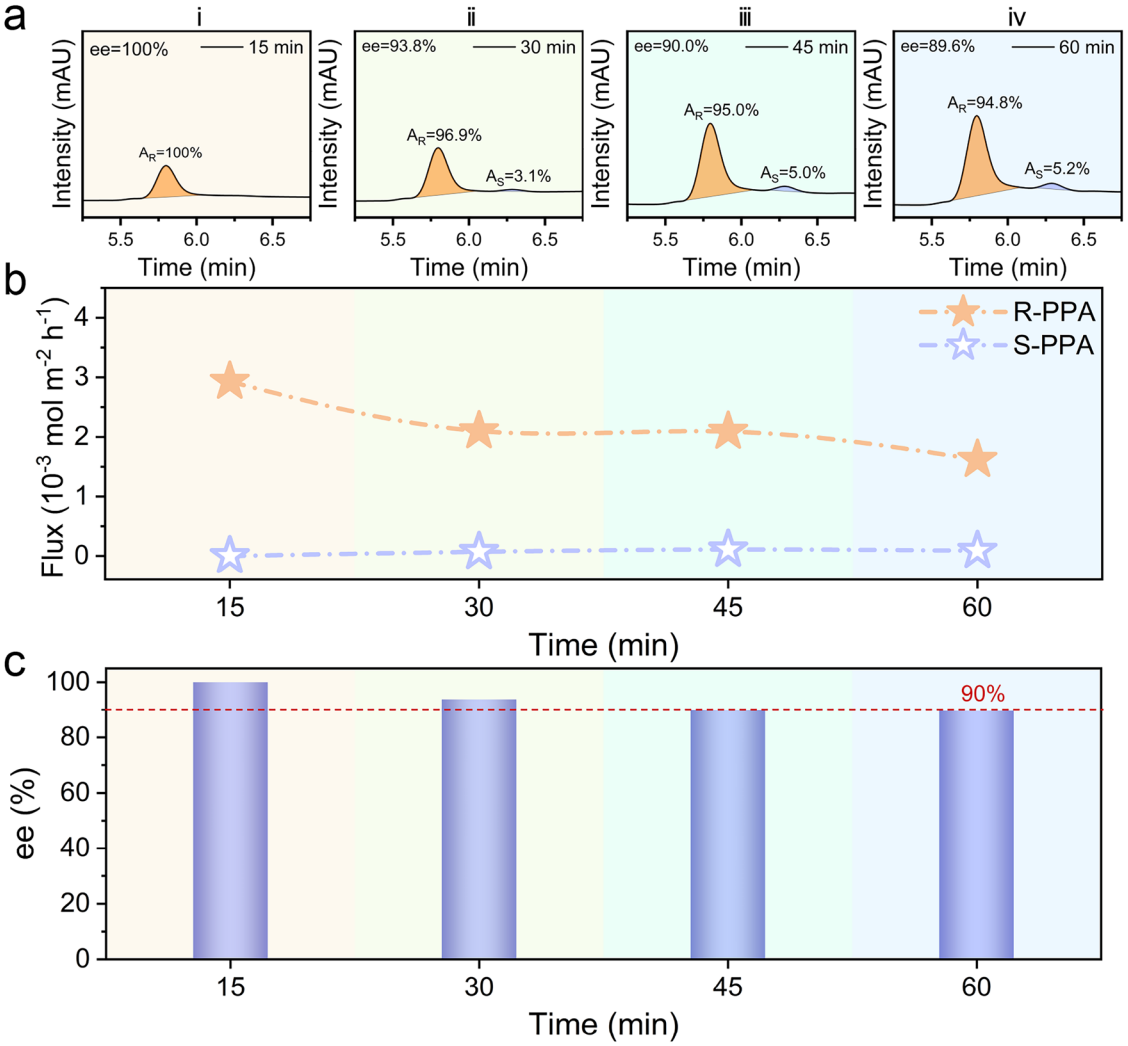

Fig. 3 | Enantioselective separation of CC3-HPABP-15% membrane at a high feed concentration. a HPLC spectra of 2-phenylpropionic acid enantiomers after separation for 15 min (i), 30 min (ii), 45 min (iii), and 60 min (iv) under 0.1 mol L^{-1} feed solution. **b** Flux of enantiomers of 2-phenylpropionic acid of the CC3-HPABP-15% membrane during 1 h. **c** Enantiomeric excess (ee) of the CC3-HPABP-15% membrane during 1 h.

phenylpropionic acid at different concentrations are shown in Fig. 5a. The flux of R-2-phenylpropionic acid rises from 9.10×10^{-4} mol m^{-2} h^{-1} to 1.62×10^{-3} mol m^{-2} h^{-1} with the increase of feed concentration from 0.001 to 0.1 mol L^{-1}, which is consistent with the expectation that flux increases with increasing driving force. However, the flux of S-2-phenylpropionic acid remains basically constant at a relatively low level with increasing feed concentration. The uniformly distributed CC3-R crystals within the membrane preferentially adsorb S-2-phenylpropionic acid and retain it in the membrane through the strong binding affinity between the chiral recognition sites and the enantiomers. Meanwhile, the non-selective diffusion of 2-phenylpropionic acid becomes noteworthy with increasing concentration gradient. As shown in Fig. 5b, the ee values of CC3-HPABP-15% membrane display an increased decline rate from 100% to 90% within 1 h, as the feed concentration increased from 0.001 to 0.1 mol L^{-1}. This is because the chiral recognition sites of CC3-R crystals within the membrane can reach saturation rapidly with increasing concentration, which results in a decrease in the enantioselectivity.

To validate the general applicability of POC-based MMMs, the enantioselective separation performance toward a wide range of chiral molecules was investigated (Supplementary Fig. 36). The results demonstrate that the CC3-HPABP-15% membrane exhibits good enantioselectivity toward racemic 2-phenylbutanoic acid, 2-(4-methylphenyl) propanoic acid, and mandelic acid, with ee values of 98.2%, 98.4%, and 90.4%, respectively (R-enantiomer in excess). The fluxes of 2-phenylbutanoic acid, 2-(4-methylphenyl) propanoic acid, and mandelic acid were 1.65×10^{-3}, 1.12×10^{-3}, and 7.70×10^{-4} mol·m^{-2}·h^{-1}, respectively.

Compared to other reported enantioselective membranes under the concentration-gradient driven, the CC3-HPABP-15% membrane exhibits a competent enantioseparation performance with the lowest ee decline rate of 0.56% h^{-1} (Fig. 5c, d and Supplementary Table 2)[18,23,26,41,46]. The POCs with a window-cavity structure act as functional enantioselective selectors and minimize the performance recession caused by interfacial defects.

Discussion

In summary, we reported homochiral POC-based MMMs for fast and selective enantioseparation. MMMs (e.g., CC3-HPABP membranes) exhibit superior enantioselective separation of racemic 2-phenylpropionic acid at a high feed concentration because of the optimal interfacial compatibility. Moreover, the CC3-HPABP-15% membrane demonstrates a long-term separation stability with inconspicuously declined ee values. Theoretical calculations reveal that the enantioselectivity stems from the specific hydrogen bonding

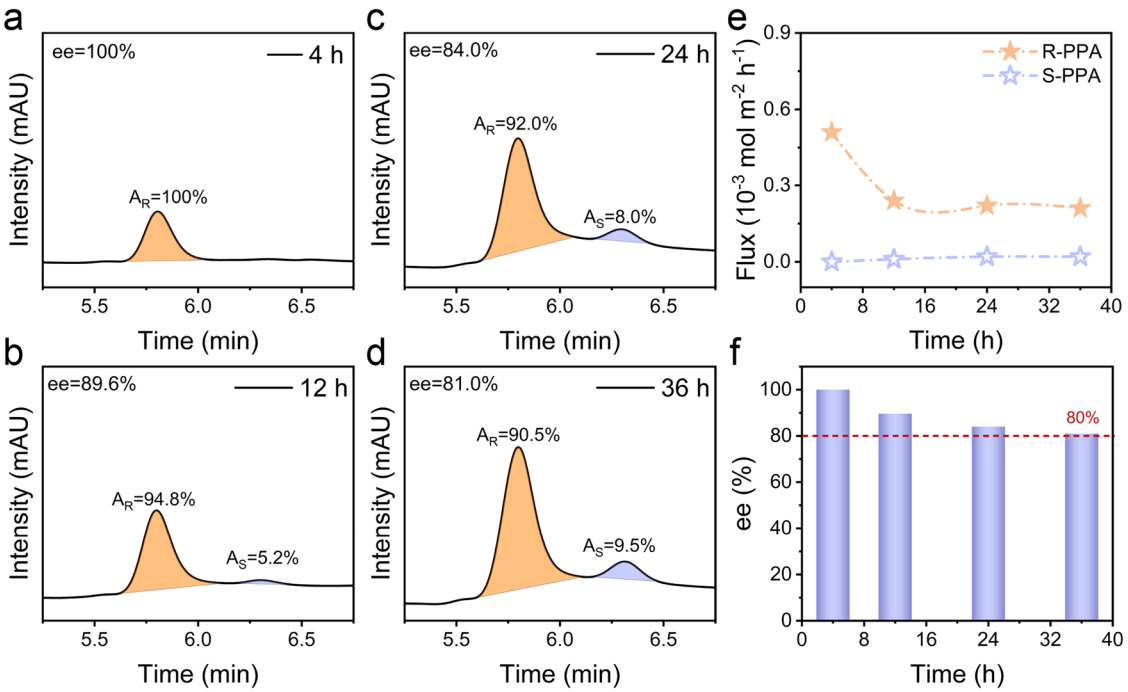

Fig. 4 | Enantioselective separation stability of CC3-HPABP-15% membrane. HPLC spectra of 2-phenylpropionic acid enantiomers after separation for **a** 4 h, **b** 12 h, **c** 24 h, and **d** 36 h under 0.001 mol L^{-1} feed solution. **e** Flux of the CC3-HPABP-15% membrane varying within 36 h. **f** Enantiomeric excess (ee) of the CC3-HPABP-15% membrane varying within 36 h.

interactions between the enantiomeric binding sites of the POCs and the enantiomers. This work reveals the imperative role of the microporous chiral environment in POCs for the enantioselective recognition, and offers new insights into the design of efficient chiral separation membranes based on homochiral POCs.

Methods

Synthesis of CC3-R

The CC3-R was synthesized as previously reported[42]. 1 g of 1,3,5-triformylbenzene and 1 g of (1R,2R)-1,2-cyclohexanediamine were dissolved in 40 mL DCM, and then 20 μL TFA was added to the solution as the catalyst. The mixture was reacted for 4 days at room temperature. Hereafter, the CC3-R crystals were collected by centrifugation and then washed with 95% ethanol/5% dichloromethane. The CC3-R crystals were finally dried under vacuum.

Synthesis of CC4-R

The CC4-R was synthesized as previously reported with slight modifications[43]. 1.6 g of (1R, 2R)-1,2-cyclopentadiamine dihydrochloride and 2.6 mL triethylamine were dissolved in 50 mL methanol. The resulting solution was added dropwise to a stirred solution of 1,3,5-triformylbenzene (1 g in 50 mL DCM). The mixture was maintained for 7 days at room temperature. Hereafter, the CC4-R crystals were collected by centrifugation and then washed with 95% methanol/5% dichloromethane. The CC4-R crystals were finally dried under vacuum.

Synthesis of CC19-R

The CC19-R was synthesized as previously reported[42]. 1 g of 2-hydroxy-1,3,5-triformylbenzene and 1 g of (1 R,2 R)-1,2-cyclohexanediamine were dissolved in 40 mL DCM, and then 20 μL TFA was added to the solution as the catalyst. The mixture was reacted for 4 days at room temperature. Hereafter, the CC19-R crystals were collected by centrifugation and then washed with diethyl ether. The CC19-R crystals were finally dried under vacuum.

Synthesis of polymer protonated poly (alkyl-biphenyl pyridinium) (HPABP)

The polymer HPABP was synthesized through the superacid-catalyzed polymerization of 4-acetylpyridine and biphenyl as previously reported[47,48]. Biphenyl (3.6 g, 15.6 mmol) and 4-acetylpyridine (2.5 g, 20.4 mmol) were dissolved in dichloromethane (CH_2Cl_2, 16.4 mL) under an ice bath. With mechanical stirring, trifluoroacetic acid (TFA, 0.8 mL) and trifluoromethanesulfonic acid (TFSA, 14 mL) were sequentially added. The ice bath was removed after 15 min, and the reactant mixture was stirred at room temperature for 48 h. The resulting dark blue viscous solution was poured into 1 mol L^{-1} $NaHCO_3$ solution, yielding a yellow product. The product was then dried in an oven at 120 °C for 12 hours to afford the final HPABP polymer.

Synthesis of POC-based mixed matrix membranes (MMMs)

POC-based MMMs were prepared as reported in the previous literature[38]. 1 g of HPABP was dissolved in a mixture of solvents (2 g of methanol and 8 g of DCM), and then 0.177 g (15 wt%) of POC crystals were added to the above solution. The mixture was stirred vigorously until completely dissolved. After that, the mixture was sonicated to expel air bubbles and then was cast to prepare a membrane on a glass plate at room temperature. In addition, to investigate the effect of POC loading on the chiral separation performance of the MMMs, membranes with different POC loadings (5 wt% and 30 wt%) were prepared under the same conditions.

Chiral separation measurement

A homemade diffusion device was used to explore the chiral separation performance of MMMs. The diffusion device consists of a feed chamber and a permeation chamber assembled side by side, the membrane is placed between the two chambers and the rubber gaskets are used to seal the connection, with an effective membrane area of 1.13 cm^2. 15 mL of racemic 2-phenylpropionic acid in ethanol was added to the feed chamber, and the same amount of pure ethanol was added to the permeation chamber, accompanied by a continuous

https://doi.org/10.1038/s41467-025-66642-7

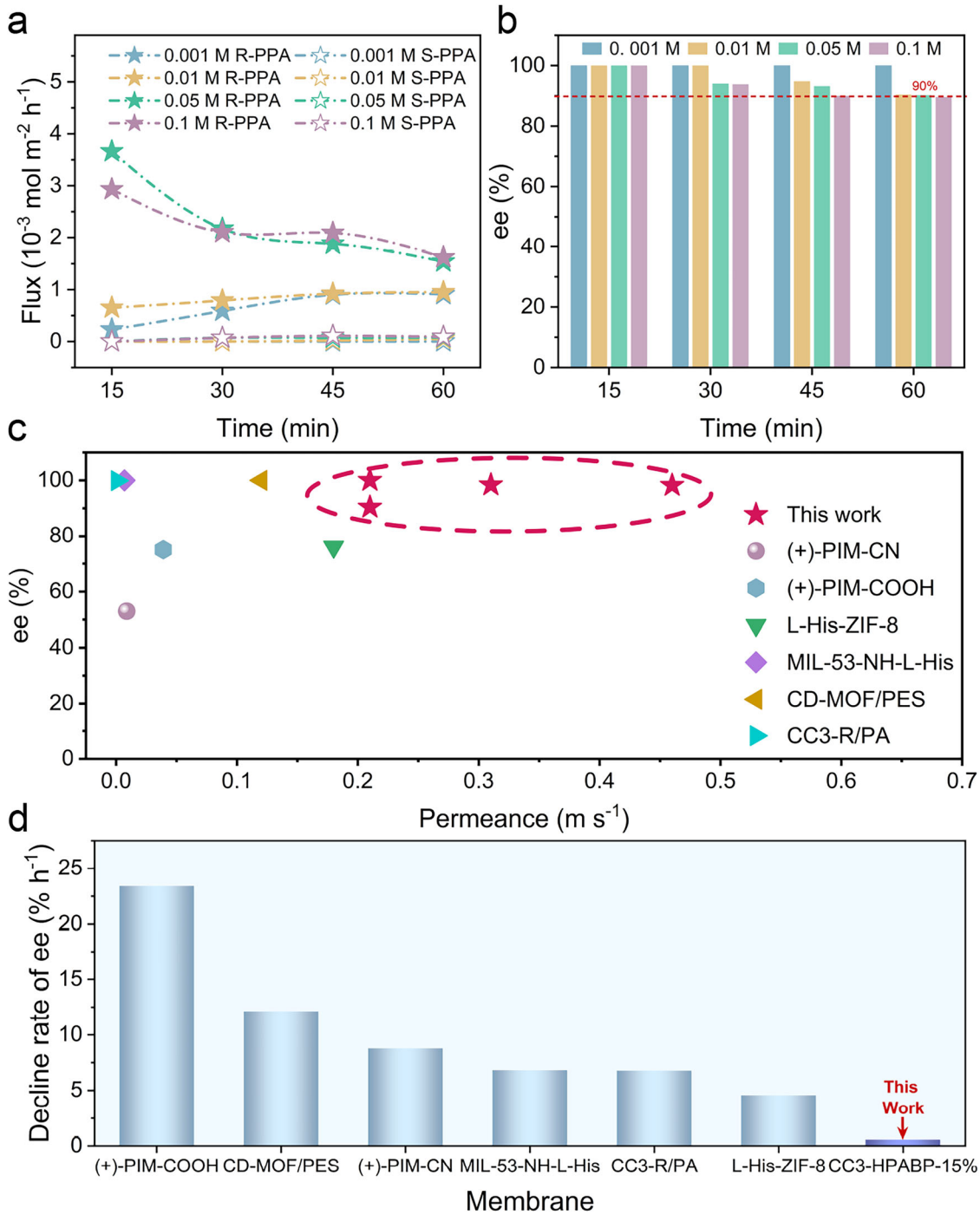

Fig. 5 | Enantioselective separation of CC3-HPABP-15% membrane under different concentration gradients. a Flux of enantiomers of 2-phenylpropionic acid of the CC3-HPABP-15% membrane under different feed concentrations. **b** Enantiomeric excess (ee) of the CC3-HPABP-15% membrane under different feed concentrations. **c** Comparison of the chiral separation performance (i.e., permeance and ee) of the CC3-HPABP-15% membrane with the reported representative enantioselective membranes under concentration gradient-driven conditions. **d** The ee decline rate comparison of CC3-HPABP-15% membrane with reported representative enantioselective membranes.

stirring using a magnetic stirring device. The racemic compound is driven under the concentration gradient to diffuse across the membrane. The analyte was collected from the permeation side and analyzed by the HPLC.

Chiral separation performance

The concentrations of 2-phenylpropionic acid enantiomers were analyzed using an Agilent 1260 Infinity II HPLC system equipped with a chiral column (Daicel CHIRALPAK® AD-H, 250×4.6, 5 μm). The mobile phase consists of n-hexane/isopropyl alcohol/trifluoroacetic acid (v/v/v = 90/10/0.1). The injection amount is 10 μL and the flow rate of the mobile phase is 1 mL min^{-1}. The analysis temperature is 35 °C and the UV-detector is set to 210 nm. A standard calibration curve was used to calculate the concentration of each enantiomer.

The enantioselectivity of chiral separation is expressed by the enantiomeric excess (ee) value. The ee value is calculated by the

equation below[49]:

$$ee(\%) = \frac{|A_R - A_S|}{A_R + A_S} \times 100\% \quad (1)$$

Where A_R and A_S represent the peak area of the R-enantiomer and S-enantiomer, respectively.

The permeation flux is calculated by the equation below[50]:

$$Flux = \frac{n}{A\Delta t} \quad (2)$$

Where n (mol) is the concentration of enantiomers in the permeate, A (m^2) is the effective membrane permeation area, and Δt (h) is the permeation time.

The permeance is calculated by the equation below:

$$Permeance = \frac{Flux}{\Delta F} \quad (3)$$

Where ΔF is the difference in driving force across the membrane (i.e., concentration difference of the feed and permeation solution).

Enantioselective adsorption of POC crystals

The enantioselective adsorption experiments were conducted by adding POCs crystals (20 mg) to the ethanol solution containing racemic 2-phenypropionic acid (5 mL, 1 mmol L^{-1}) under stirring at room temperature. After 24 hours, the solid samples of POC crystals selectively bound with R- or S-2-phenypropionic acid were filtered out. The remaining filtrate solution was analyzed by HPLC.

Density functional theory (DFT) calculations

The density functional theory (DFT) calculations were performed using a Dmol3 module of Material Studio[51]. The generalized gradient approximation (GGA) method with Perdew-Burke-Ernzerhof (PBE) function was employed to describe the interactions between the core and electrons[52]. The force and energy convergence criteria were set to 0.002 Ha $Å^{-1}$ and 10^{-5} Ha, respectively.

The binding energy (ΔE) was calculated as:

$$\Delta E(eV) = 27.212 \times [E_{total}(Ha) - E_1(Ha) - E_2(Ha)] \quad (4)$$

where the E_{total} is the energy of the optimized system; E_1 is the energy of R-2-phenylpropionic acid or S-2-phenylpropionic acid; E_2 is the energy of CC3-R, CC4-R, or CC19-R.

Molecular dynamic (MD) simulations

Molecular dynamics (MD) simulations were carried out with the Forcite module[53]. In describing the interactions within the simulations, van der Waals forces were represented using an atom-based summation approach, with the Lennard-Jones (L-J) model specifying them up to a cut-off distance of 12 Å. Meanwhile, electrostatic interactions between the guest molecules being studied and the overarching structure were depicted using the Ewald summation method. The simulation was executed over a span of 500 ps with a 1 fs time increment. By evaluating the mean square displacement (MSD) over time and fitting these values, the diffusion coefficient (D) was calculated according to the following equation[54]:

$$D = \frac{1}{6Na} \lim_{t\to\infty} \frac{d}{dt} \sum_{i=1}^{Na} [r_i(t) - r_i(0)]^2 \quad (5)$$

where $r_i(0)$, $r_i(t)$ are the position vectors of the i_{th} molecule from time 0 to t.

Data availability

The authors confirm that the data supporting the findings of this study are available within the article and its supplementary information. All data are available from the corresponding author upon request.

References

1. Brooks, W. H. et al. The significance of chirality in drug design and development. *Curr. Top. Med. Chem.* **11**, 760–770 (2011).
2. Jeschke, P. Current status of chirality in agrochemicals. *Pest Manag. Sci.* **74**, 2389–2404 (2018).
3. D'Orazio, G. et al. Chiral separations in food analysis. *TrAC Trends Anal. Chem.* **96**, 151–171 (2017).
4. Afonso, C. A. M. & Crespo, J. G. Recent advances in chiral resolution through membrane-based approaches. *Angew. Chem. Int. Ed.* **43**, 5293–5295 (2004).
5. Xie, R. et al. Membranes and membrane processes for chiral resolution. *Chem. Soc. Rev.* **37**, 1243–1263 (2008).
6. Yu, C. et al. Advances in membrane-based chiral separation. *Coord. Chem. Rev.* **495**, 215392 (2023).
7. Wang, Y. et al. Graphite phase carbon nitride based membrane for selective permeation. *Nat. Commun.* **10**, 2500 (2019).
8. Xue, M. et al. Emerging functional chiral microporous materials: synthetic strategies and enantioselective separations. *Mater. Today* **19**, 503–515 (2016).
9. Lu, Y. et al. Emerging homochiral porous materials for enantiomer separation. *Adv. Funct. Mater.* **31**, 2101335 (2021).
10. Sun, Z. et al. Nanoporous materials for chiral resolution. *Coord. Chem. Rev.* **425**, 213481 (2020).
11. Wu, X. et al. Chiral BINOL-based covalent organic frameworks for enantioselective sensing. *J. Am. Chem. Soc.* **141**, 7081–7089 (2019).
12. Han, Z. et al. Chiral linker installation in a metal-organic framework for enantioselective luminescent sensing. *J. Am. Chem. Soc.* **146**, 15446–15452 (2024).
13. Liu, Y. et al. Engineering homochiral metal-organic frameworks for heterogeneous asymmetric catalysis and enantioselective separation. *Adv. Mater.* **22**, 4112–4135 (2010).
14. Xu, J. et al. Functional covalent organic frameworks' microspheres synthesized by self-limited dynamic linker exchange for stationary phases. *Adv. Mater.* **36**, 2406256 (2024).
15. Qian, H. et al. Bottom-up synthesis of chiral covalent organic frameworks and their bound capillaries for chiral separation. *Nat. Commun.* **7**, 12104 (2016).
16. Han, X. et al. Chiral induction in covalent organic frameworks. *Nat. Commun.* **9**, 1294 (2018).
17. Han, Z. et al. Cation-induced chirality in a bifunctional metal-organic framework for quantitative enantioselective recognition. *Nat. Commun.* **10**, 5117 (2019).
18. Chan, J. et al. Incorporation of homochirality into a zeolitic imidazolate framework membrane for efficient chiral separation. *Angew. Chem. Int. Ed.* **57**, 17130–17134 (2018).
19. Wang, W. et al. A homochiral metal-organic framework membrane for enantioselective separation. *Chem. Commun.* **48**, 7022–7024 (2012).
20. Zhang, S. et al. Chiral covalent organic framework packed nanochannel membrane for enantioseparation. *Angew. Chem. Int. Ed.* **61**, e202204012 (2022).
21. Chen, Y. et al. In situ fabrication of chiral covalent triazine frameworks membranes for enantiomer separation. *J. Chromatogr. A* **1654**, 462475 (2021).
22. Chen, T. et al. Robust homochiral polycrystalline metal-organic framework membranes for high-performance enantioselective separation. *J. Am. Chem. Soc.* **146**, 14433–14438 (2024).
23. Lu, Y. et al. Cyclodextrin metal-organic framework-polymer composite membranes towards ultimate and stable enantioselectivity. *J. Membr. Sci.* **620**, 118956 (2021).

24. Das, S. et al. Chiral recognition and separation by chirality-enriched metal-organic frameworks. *Angew. Chem. Int. Ed.* **57**, 8629–8633 (2018).
25. Yuan, C. et al. Nanochannels of covalent organic frameworks for chiral selective transmembrane transport of amino acids. *J. Am. Chem. Soc.* **141**, 20187–20197 (2019).
26. Lu, Y. et al. Homochiral MOF-polymer mixed matrix membranes for efficient separation of chiral molecules. *Angew. Chem. Int. Ed.* **58**, 16928–16935 (2019).
27. Wang, H. et al. Membrane adsorbers with ultrahigh metal-organic framework loading for high flux separations. *Nat. Commun.* **10**, 4204 (2019).
28. Zhang, Y. et al. Challenges and recent advances in MOF-polymer composite membranes for gas separation. *Inorg. Chem. Front.* **3**, 896–909 (2016).
29. Zhu, G. et al. Molecularly mixed composite membranes for advanced separation processes. *Angew. Chem. Int. Ed.* **58**, 2638–2643 (2019).
30. Holst, J. R. et al. Porous organic molecules. *Nat. Chem.* **2**, 915–920 (2010).
31. Jones, J. T. A. et al. Modular and predictable assembly of porous organic molecular crystals. *Nature* **474**, 367–371 (2011).
32. Song, Q. et al. Porous organic cage thin films and molecular-sieving membranes. *Adv. Mater.* **28**, 2629–2637 (2016).
33. Zhang, J. et al. Recent advances of application of porous molecular cages for enantioselective recognition and separation. *J. Sep. Sci.* **43**, 134–149 (2020).
34. Wang, Z. et al. Porous organic nanocages CC3 and CC3-OH for chiral gas chromatography. *Acs Appl. Nano Mater.* **3**, 479–485 (2020).
35. Liu, Y. et al. Porous organic cage for enantiomeric fluorescence recognition of amino acid and hydroxy acid. *Luminescence* **36**, 2022–2027 (2021).
36. Hasell, T. et al. Chirality as a tool for function in porous organic cages. *Nanoscale* **9**, 6783–6790 (2017).
37. Cui, D. et al. Chiral self-sorting and guest recognition of porous aromatic cages. *Nat. Commun.* **13**, 4011 (2022).
38. Xu, T. et al. Scalable and interfacial gap-free mixed matrix membranes for efficient anion separation. *AIChE J.* **70**, e18242 (2024).
39. Chen, L. et al. Separation of rare gases and chiral molecules by selective binding in porous organic cages. *Nat. Mater.* **13**, 954–960 (2014).
40. Kewley, A. et al. Porous organic cages for gas chromatography separations. *Chem. Mater.* **27**, 3207–3210 (2015).
41. Wang, F. et al. A homochiral porous organic cage-polymer membrane for enantioselective resolution. *Adv. Mater.* **36**, 2400709 (2024).
42. Xu, T. et al. Insight into ion transport in discrete frameworks of porous organic cage membranes. *Ind. Eng. Chem. Res.* **62**, 717–724 (2023).
43. Mitra, T. et al. A soft porous organic cage crystal with complex gas sorption behavior. *Chem. Eur. J.* **17**, 10235–10240 (2011).
44. Qu, K. et al. Electrostatic-induced crystal-rearrangement of porous organic cage membrane for CO_2 capture. *Angew. Chem. Int. Ed.* **61**, e202205481 (2022).
45. Zhang, Q. et al. Mixed-matrix membranes with soluble porous organic molecular cage for highly efficient C_3H_6/C_3H_8 separation. *J. Membr. Sci.* **611**, 118288 (2020).
46. Weng, X. et al. Chiral polymers of intrinsic microporosity: selective membrane permeation of enantiomers. *Angew. Chem. Int. Ed.* **54**, 11214–11218 (2015).
47. Jin, Y. et al. High-performance poly(biphenyl acetylpyridine) and poly(ether ketone cardo) blend membranes for high-temperature polymer electrolyte membrane fuel cells. *Macromol. Mater. Eng.* **307**, 2200300 (2022).
48. Cetina-Mancilla, E. et al. Well-defined, linear, wholly aromatic polymers with controlled content and position of pyridine moieties in macromolecules from one-pot, room temperature, metal-free step-polymerizations. *Polym. Chem.* **11**, 6194–6205 (2020).
49. Li, Q. et al. Preparation and characterization of $Ni_2(mal)_2(bpy)$ homochiral MOF membrane. *Asia-Pac. J. Chem. Eng.* **11**, 60–69 (2016).
50. Huang, K. et al. Fabrication of homochiral metal-organic framework membrane for enantioseparation of racemic diols. *AIChE J.* **59**, 4364–4372 (2013).
51. Zhang, J. et al. Mechanism of hydrodeoxygenation (HDO) in anisole decomposition over metal loaded bronsted acid sites: density functional theory (DFT) study. *Mol. Catal.* **454**, 30–37 (2018).
52. Saeed, Z. M. et al. Crystal engineering of binary organic eutectics: significant improvement in the physicochemical properties of polycyclic aromatic hydrocarbons via the computational and mechanochemical discovery of composite materials. *Cryst. Growth Des.* **21**, 4151–4161 (2021).
53. Gholizadeh, R. & Wang, Y. Molecular dynamics simulation of the aggregation phenomenon in the late stages of silica materials preparation. *Chem. Eng. Sci.* **184**, 62–71 (2018).
54. Lu, J. et al. Molecular dynamics simulations of interfacial interactions between small nanoparticles during diffusion-limited aggregation. *Appl. Surf. Sci.* **357**, 1114–1121 (2015).

Acknowledgements

This work was supported by the National Natural Science Foundation of China (22278387, 22478372, 22108267, 22378001), the Strategic Priority Research Program of the Chinese Academy of Sciences (XDB0450000). This work was partially carried out at the Instruments Center for Physical Science, University of Science and Technology of China.

Author contributions

Y.L. contributed to the data curation, formal analysis, investigation, methodology, and writing the original draft. Z.L., D.Z., Y.X., and B.W. contributed to the data curation and investigation. T.X. (Tingting Xu), X.L., and T.X. (Tongwen Xu) contributed to conceptualization, project administration, and supervision. All authors contributed to the review and editing of the manuscript.

Competing interests

The authors declare no competing interests.

Additional information

Supplementary information The online version contains supplementary material available at https://doi.org/10.1038/s41467-025-66642-7.

Correspondence and requests for materials should be addressed to Tingting Xu, Xingya Li or Tongwen Xu.

Peer review information *Nature Communications* thanks the anonymous reviewers for their contribution to the peer review of this work. A peer review file is available.